

ISO–SWS observations of pure rotational H₂O absorption lines toward Orion–IRc2^{*}

C.M. Wright^{1,2}, E.F. vanDishoeck¹, J.H. Black³, H. Feuchtgruber^{4,5}, J. Cernicharo⁶, E. González-Alfonso^{6,7}, and Th. deGraauw⁸

¹ Leiden Observatory, P.O. Box 9513, 2300 RA Leiden, The Netherlands

² School of Physics, University College, Australian Defence Force Academy, University of New South Wales, Canberra ACT 2600, Australia

³ Onsala Space Observatory, Chalmers University of Technology, 43992 Onsala, Sweden

⁴ ISO–SOC, ESA Astrophysics Division, P.O. Box 50727, 28080 Villafranca/Madrid, Spain

⁵ Max-Planck-Institut für Extraterrestrische Physik, Postfach 1603, 85740 Garching bei München, Germany

⁶ CSIC–IEM, Serrano 121, 28006 Madrid, Spain

⁷ Universidad de Alcalá de Henares, Dept. de Física, Campus Universitario, 28871 Alcalá de Henares, Madrid, Spain

⁸ SRON, P.O. Box 800, 9700 AV Groningen, The Netherlands

Received 12 August 1999 / Accepted 14 March 2000

Abstract. First detections of thermal water vapor absorption lines have been made toward Orion IRc2 using the *Short Wavelength Spectrometer* (SWS) on board the *Infrared Space Observatory* (ISO). Grating spectra covering wavelengths 25–45 μm yield 19 pure rotational lines, originating from energy levels 200–750 K above ground. Fabry-Perot spectra of 5 transitions resolve the line profiles and reveal the H₂O gas kinematics. The fact that all lines are seen in absorption is in striking contrast with data from the ISO *Long Wavelength Spectrometer* (LWS), where the H₂O lines appear in emission. At least one line displays a P-Cygni type profile, which suggests that the water is located in an expanding shell centered on or near IRc2. The expansion velocity is 18 km s⁻¹, in agreement with the value inferred from H₂O maser observations by Genzel et al. (1981). Because the continuum is intense and likely formed in or near the water-containing gas, the excitation of the observed transitions is dominated by radiative processes. A simple, generalised curve-of-growth method is presented and used to analyze the data. A mean excitation temperature of 72 K and a total H₂O column density of $1.5 \times 10^{18} \text{ cm}^{-2}$ are inferred, each with an estimated maximum uncertainty of 20%. Combined with the H₂ column density derived from ISO observations of the pure rotational H₂ lines, and an assumed temperature of 200–350 K, the inferred H₂O abundance is $2\text{--}5 \times 10^{-4}$ in the warm shocked gas. This abundance is similar to that found recently by Harwit et al. (1998) toward Orion using data from the LWS, but higher than that found for most other shocked regions by, for example, Liseau et al. (1996).

Key words: stars: pre-main sequence – ISM: abundances – ISM: individual objects: Orion IRc2 – ISM: jets and outflows – ISM: molecules – infrared: ISM: lines and bands

1. Introduction

Water is one of the prime species for probing the interaction between young stars and their surroundings, both in terms of its abundance and its peculiar excitation. In high temperature gas, appropriate to shocks and hot cores for instance, all of the oxygen not locked up in CO is predicted to be driven into H₂O at temperatures above 230 K by the $\text{O} + \text{H}_2 \rightarrow \text{OH} + \text{H}$ and $\text{OH} + \text{H}_2 \rightarrow \text{H}_2\text{O} + \text{H}$ reactions, resulting in very bright H₂O lines (e.g., Hollenbach & McKee 1979, Neufeld & Melnick 1987, Kaufman & Neufeld 1996, Charnley 1997). In contrast, the H₂O abundance may be at least two orders of magnitude lower in surrounding colder gas (e.g., Zmuidzinas et al. 1995). In addition to collisions, the H₂O excitation and line profiles can be strongly affected by mid- and far-infrared radiation from warm dust (e.g., Phillips et al. 1978, Takahashi et al. 1983, 1985), providing detailed information on the physical parameters of the gas and its location with respect to the radiation sources.

Interstellar water has been difficult to detect, apart from its presence as an ice mantle on dust grains or through its maser emission, owing to the severe telluric absorption encountered at Earth-based observatories. Nevertheless, over the last twenty years, many searches for lines of gas-phase H₂O and its isotopomers have been made from the ground and airborne altitudes, in particular toward Orion (e.g., Waters et al. 1980, Phillips et al. 1978, Jacq et al. 1990, Wannier et al. 1991, Cernicharo et al. 1994, Zmuidzinas et al. 1995, Tauber et al. 1996, Timmermann et al. 1996, Gensheimer et al. 1996, Cernicharo et al. 1999a,b). However, due to the choice of line, wavelength and beam size, different components are often probed, whilst many

Send offprint requests to: C.M. Wright (wright@ph.adfa.edu.au)

^{*} Based on observations with ISO, an ESA project with instruments funded by ESA Member States (especially the PI countries: France, Germany, The Netherlands and the United Kingdom) and with the participation of ISAS and NASA.

ground-based observations refer to masing lines, for which sophisticated shock and maser models are required in order to extract physical parameters.

One of the major aims of the *Infrared Space Observatory* (ISO) mission has been the routine measurement of thermal gas-phase water lines, and their use as diagnostics of the chemical and physical conditions within molecular clouds. Far-infrared pure rotational H₂O emission lines in the 50–200 μm wavelength range have been detected with the *Long Wavelength Spectrometer* (LWS) of ISO in a number of star-forming regions (e.g., Liseau et al. 1996, Ceccarelli et al. 1998), including Sgr B2 (Cernicharo et al. 1997a) and Orion (Cernicharo et al. 1997b, 1999a; Harwit et al. 1998). Additionally, van Dishoeck & Helmich (1996), van Dishoeck (1998) and Dartois et al. (1998) have observed absorption around 6 μm in the $\nu_2=1-0$ band toward a number of deeply embedded, massive young stars. Typical H₂O abundances of 10^{-5} with respect to H₂ have been derived from these data. Similar observations have recently been reported for Orion BN/IRc2 by van Dishoeck et al. (1998) and González-Alfonso et al. (1998), although in this case emission is also detected. Wright et al. (1997) have however shown that the detection of the corresponding pure rotational lines at ~ 30 –200 μm in most sources observed at 6 μm is still difficult. The observations of Orion-IRc2 presented here form a notable exception.

Many of the earlier searches for H₂O lines have been performed toward the BN/IRc2 complex of infrared sources in Orion, because of the extraordinary brightness of many atomic and molecular lines in this region compared with other clouds (e.g., Genzel & Stutzki 1989, Blake 1997). See van Dishoeck et al. (1998) and references therein for a detailed description of the geometry and the diverse range of physical phenomena in this region. In this paper we present the first detection of numerous pure rotational water lines in absorption toward IRc2 in the 25–45 μm interval with the *Short Wavelength Spectrometer* (SWS) (de Graauw et al. 1996) on board ISO. Some of these lines have been velocity resolved with the Fabry-Perot, enabling direct information on the location of the absorbing gas to be inferred. These data complement the earlier ground-based data, as well as observations of pure rotational lines with the LWS obtained by Cernicharo et al. (1997b, 1999a) and Harwit et al. (1998) in a much larger beam.

Our interpretation of the ISO spectra of Orion IRc2 suggests that the 25–45 μm H₂O spectrum originates in a region where the intrinsically strong lines couple efficiently to an intense continuum. In principle, the formation of such a spectrum should be described for a stratified atmosphere in which lines and continuum are treated self-consistently. We show here that the observed features of the spectrum can be described well by a simple “generalised curve-of-growth”, which includes the effects of coupling to a strong continuum. In the following we describe our observations and present our results, followed by a discussion of the location of the absorbing water vapour, its excitation and finally its abundance.

2. Observations and data reduction

2.1. Observations

A complete grating scan from 2.4–45.3 μm using the maximum spectral resolution SWS06 observing mode was made on September 6 1997 (revolution 660) centered at $\alpha(2000) = 05^{\text{h}}35^{\text{m}}14.2^{\text{s}}$, $\delta(2000) = -05^{\circ}22'31.5''$, which is about 3'' W and 1'' S of the IRc2 position quoted by Downes et al. (1981). The long axis of the ISO-SWS aperture was oriented at 172.81° E of N. The aperture size varies from $14'' \times 20''$ at 2.4–12 μm , to $14'' \times 27''$ at 12–27.5 μm , $20'' \times 27''$ at 27.5–29 μm and $20'' \times 33''$ at 29–45.2 μm . A further SWS06 scan was made from 26.3 to 45.2 μm in revolution 826 (February 19 1998) with the long axis oriented at 165.79° E of N. The SWS beam includes both IRc2 and BN, but not “peak 1” or “peak 2” of shocked H₂ (Beckwith et al. 1978).

The resolving power of the ISO-SWS grating, $\lambda/\Delta\lambda$, varies from about 1000–2500, implying that the observed line profiles are not resolved and that little velocity information can be obtained to help disentangle the various components which are known to exist toward IRc2. For this reason, follow-up observations of a selection of H₂O lines were obtained using the Fabry-Perot SWS07 observing mode in revolutions 823 and 831 (February 16 and 24 1998). Five 250 km s⁻¹ scans were made across each line. The resolving power is of order 30 000, corresponding to a velocity resolution of 10 km s⁻¹, and the aperture long axis was oriented at 164.14° and 168.46° E of N on the two dates. The aperture size is $10'' \times 39''$ and $17'' \times 40''$ for wavelengths below and above 26 μm respectively. During the revolution 831 observation the wavelength interval between 5.3 and 7.0 μm was simultaneously scanned by the SWS grating. Within this region are several H₂ lines (0–0 S(7), S(6) and S(5)), and H₂O solid state ice and H₂O gas phase $\nu_2=1-0$ features.

2.2. Data reduction

Data reduction was carried out on the Standard Processed Data file from the Off Line Processing system (OLPv6.1.1 for revolution 660 and OLPv6.3.2 for revolutions 823, 826 and 831), using standard routines within the SWS Interactive Analysis package up to the Auto Analysis Result (AAR) stage. The dark current subtraction was performed interactively for the grating data, but not for the FP data. The most up-to-date calibration files available for wavelength, flux and relative spectral responsivity were used. Even so, there is at least one instrumental artefact in our grating spectra, at 33 μm , due to structure in the relative spectral response calibration file (RSRF).

The high continuum flux encountered in band 4 of the SWS grating (29–45 μm), and the finite response time of the detectors, led to significant memory and response effects near the band edges, at positions of important water and OH lines, and so necessitated a non-standard up-down scan correction. For the SWS an “up” (“down”) scan proceeds toward increasing (decreasing) grating positions but decreasing (increasing) wavelengths. Since the up scan precedes the down scan, in high flux cases it is usually the down scan which is deemed to have the more

reliable spectral shape, since by that time the instrument has settled down. Indeed, this was the case in the long-wavelength portion (41–45 μm) of our spectra, so that the up scan was corrected to approximately the same shape as the down scan. On the other hand, the short-wavelength portion (29–33 μm) of the down scan of our spectra had a peculiar concave shape, which did not match cleanly (in terms of *shape*) to band 3e, which in turn matched cleanly with band 3d. This was true for both the revolution 660 and 826 data sets. In this case therefore the down scan was corrected to have a similar shape to the up scan. The up-down correction obviously entailed splitting the band 4 data into two segments (29–37 μm and 37–45 μm), but this produced a more reliable spectral shape at both ends, e.g. allowing the continuum on either side of the 45.1 μm water line to be determined, and the 28.940 and 28.914 μm OH and H₂O 4₄₀ – 3₁₃ lines to be partially resolved.

Following the AAR stage, further data processing, such as flatfielding, sigma clipping and rebinning, was performed using software in the SWS IA package. For instance, for both the grating and FP cases the individual detector scans have been brought to a common flux level using an n^{th} degree polynomial ($n = 0, 1, 2$ or 3) fit to a reference spectrum which may either be the median of the down scans (e.g. grating band 3), the median of both the up and down scans (e.g. the up-down corrected grating band 4), or the mean of all scans (e.g. the Fabry-Perot data). The data have subsequently been sigma clipped such that any points lying more than 3 sigma outside of the average of all data within a bin of width equal to the theoretical spectral resolution have been discarded. The final step in producing a spectrum involves rebinning the much over-sampled data using the mean within a bin which is again equal to the theoretical resolution.

In the case of the 25.94 μm FP scans it was observed that glitches and their associated tails, which had not been flagged as bad data by the pipeline, contributed significant noise to the final spectrum. In this instance an interactive glitch and tail correction was performed before flatfielding, sigma clipping and rebinning. As noted by Schaeidt et al. (1996) and Heras (1997) the photometric accuracies of the SWS grating band 4 (where most of our water detections occur) and Fabry-Perot are 30% and 40% respectively. However, our observed line equivalent widths, being ratios of the line area over adjacent continuum, will be more accurate than this. The accuracy of the grating wavelength calibration is 1/10–1/5 of a resolution element, whilst that of the Fabry-Perot is of order 10^{-4} μm , or about 1 km s^{-1} (Valentijn et al. 1996; Feuchtgruber et al. 1997).

3. Results

In Fig. 1 the SWS grating spectrum in the 25–45 μm range is presented for the revolution 660 data, with the position and identification of features marked. The data consist of spectral segments from bands 3d, 3e and 4, for which “jumps” in the flux were observed due to the different aperture sizes. However, for display purposes small shifts, of order a few thousand Jy (i.e. a few percent), have been applied to produce a continuous spectrum. Clearly marked in Fig. 1 are 19 absorption lines arising from

pure rotational levels in both the ortho- (o) and para- (p) species of H₂O. In the few cases where the plot scale makes the line difficult to see in Fig. 1, we present close-ups in Fig. 2. The lines in this wavelength region originate from highly-excited states, with excitation energies of the lower levels $hcE_l/k = 200$ –750 K, and the upper levels up to 1200 K. The strongest absorptions come from levels belonging to the backbone of the energy ladder. Among the highest levels seen is the upper state of the 7₂₅ – 6₁₆ transition at 29.8367 μm , involving the upper level (6₁₆) of the well-known 22 GHz H₂O maser line (Cheung et al. 1969). Indeed, many of the levels from which absorption is seen are also upper levels of either known or suspected maser transitions (Neufeld & Melnick 1991). It is shown below based on velocity considerations that our lines probably arise in the same region where the masers are situated, indicating that our observations may form a useful data set for studying the maser pump mechanism.

A sub-set of 5 of the 19 lines was chosen to be observed with the Fabry-Perot. These spectra are shown in Fig. 3. In one case (4₃₂ – 3₀₃ 40.69 μm) and possibly a second (5₄₁ – 4₃₂ 43.89 μm), two velocity components are detected, one in absorption and the other in emission. A modulation in the baselines, due to the tracking of the Fabry-Perot transmission function across the region of the peak of the grating instrumental profile, has been modelled in terms of two parameters, the grating spectral resolution and the shift between the two response functions. The spectra shown in Fig. 3 have been corrected for this tracking pattern. Also shown in Fig. 3 is the grating spectrum from 5.3–7.0 μm obtained from these new data. It is consistent with that already observed by van Dishoeck et al. (1998) and González-Alfonso et al. (1998).

Table 1 presents an overview of our observations for the Revolution 660 data, including the rest wavelength, upper and lower levels, and equivalent widths $W = c W_\lambda / \lambda$ in units of Doppler velocity (km s^{-1}), where W_λ is the line equivalent width in wavelength units. The superscripts on W refer to the observed and calculated equivalent widths, the latter derived from a generalised curve-of-growth analysis to be described in Sect. 4.2. Table 1 also contains the results for three pure rotational OH lines detected in absorption in our spectra. All derived quantities were calculated from unshifted spectral segments. Fig. 4(a) presents our results graphically, in the form of a standard population diagram (Goldsmith & Langer 1999), where the column density in the lower level has been determined using the formula $N_\ell = (8\pi c W_\lambda g_\ell) / (\lambda^4 A_{ul} g_u)$, where g_ℓ and g_u are the statistical weights of the lower and upper levels, A_{ul} is the Einstein A -coefficient in s^{-1} and W_λ is the equivalent width. This formula is only strictly valid for optically thin lines, and under the assumption that the upper levels are not significantly populated. The error bars represent a 30% uncertainty, so that the scatter in the data is clearly larger than any systematic or statistical uncertainties. Although there is a clear trend in the data, this scatter already hints that a more detailed analysis is required to obtain a reliable total H₂O column density. Such an analysis, in the form of a generalised curve-of-growth, is presented in Sect. 4.2.

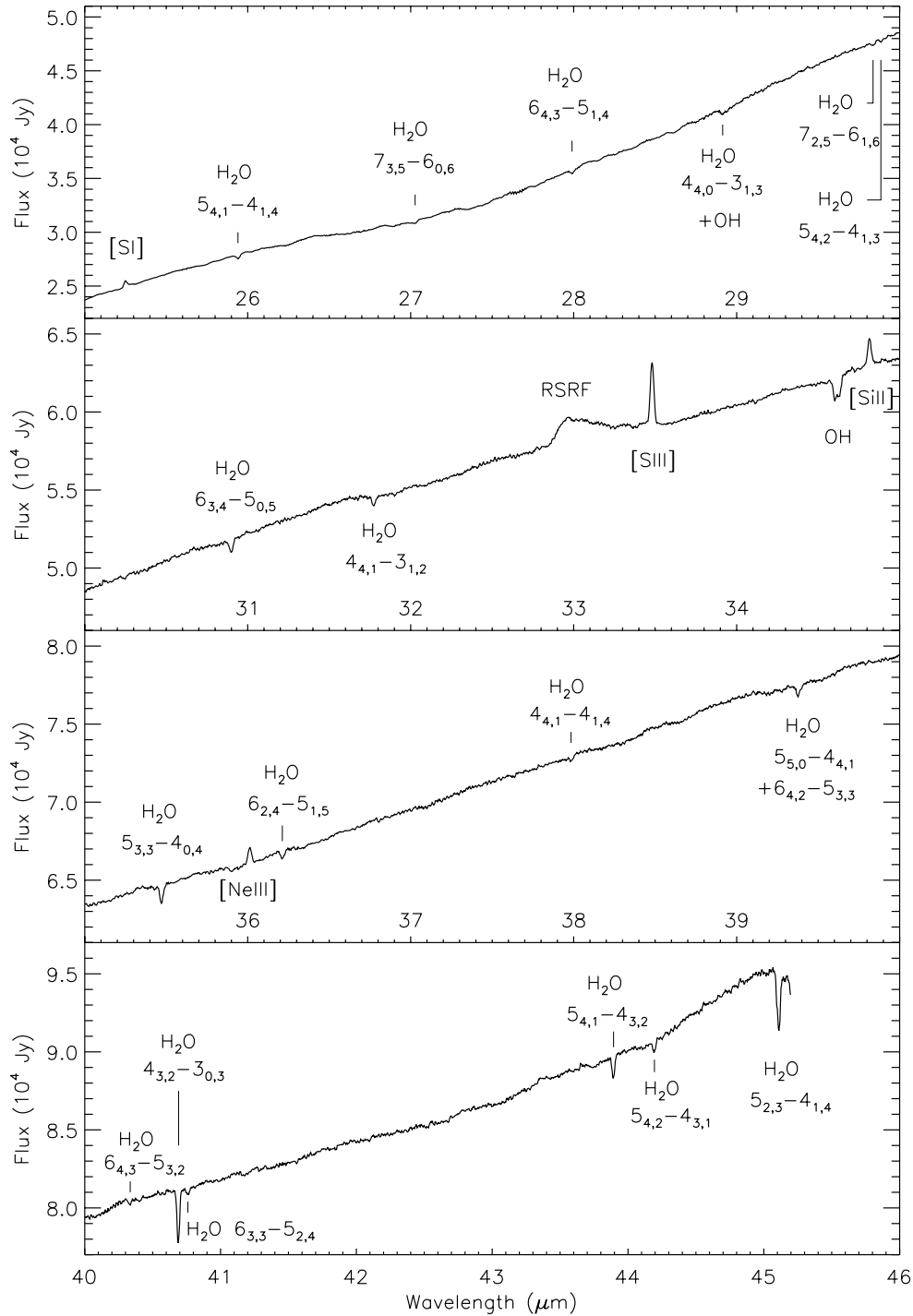


Fig. 1. ISO-SWS 25–45 μm grating spectrum toward Orion IRc2. The principal absorption and emission features are indicated. The data within bands 3d, 3e and 4 have been shifted so that they join continuously at the band edges. The feature marked RSRF is an instrumental artefact due to structure in the relative spectral response calibration file.

Almost all lines listed in Table 1 at 27.5–45.2 μm are visible in both the Revolution 660 and 826 spectra, and their measured equivalent widths agree within 30% in the majority of cases. See Fig. 4(a), where both data sets are presented graphically. We present only the Revolution 660 data in Table 1 because the data from that revolution are of a better quality, and also only 15 of the 19 lines were observed in Revolution 826 due to the shorter wavelength scan range. The fact that the pure rotational H₂O and OH lines observed with the SWS occur in absorption is in strong

contrast with the lines seen with the LWS, which are mostly in emission (e.g., Harwit et al. 1998). Since the LWS lines arise in levels with similar excitation energies at wavelengths where the continuum flux is comparable to that in the SWS range, this suggests that most of the mid-infrared continuum and H₂O absorption originate in a small region of size comparable to the SWS beam. In the almost order-of-magnitude larger area of the LWS beam, even more of the absorption is probably filled in by large-scale emission from more extended, lower excitation

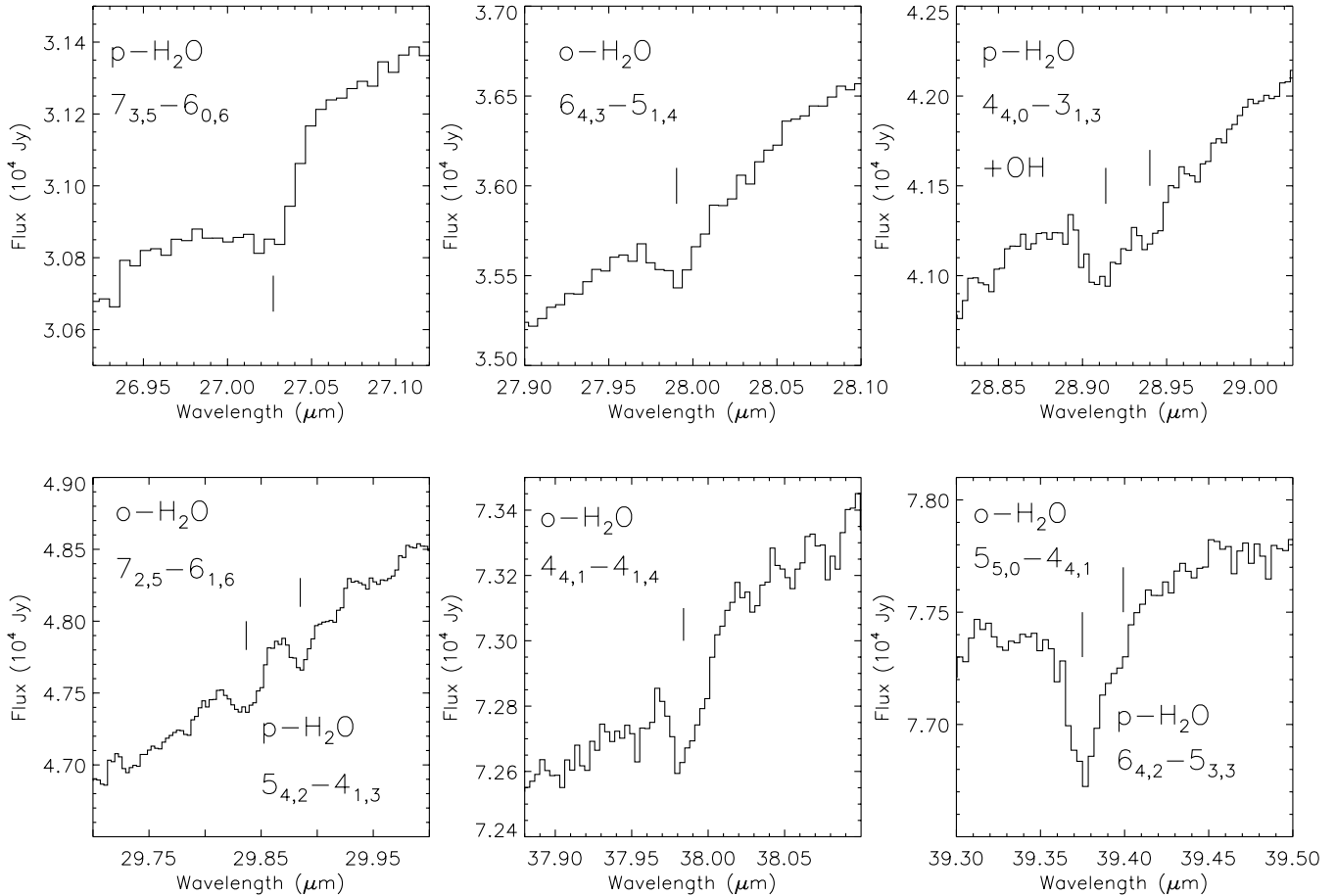


Fig. 2. Close-ups of several of the H₂O absorption lines shown in Fig. 1. The rest wavelength of each line is indicated by a tick mark. The p-H₂O 6_{4,2}-5_{3,3} 39.3992 μm line is visible as a shoulder on the deeper o-H₂O 5_{5,0}-4_{4,1} 39.3749 μm line.

shocked gas. The qualitative change in the character of the water spectrum is thus probably a result of effects of both geometry (beam-filling) and radiative transfer.

The small differences in equivalent widths found from the grating and Fabry-Perot spectra are due to uncertainties in the calibration and varying beam shapes, which may couple differently to the complex source structure. The continuum radiation at 25–45 μm is produced by extended dust emission over a ~30'' region centered near IRc2, in contrast with the situation at ~6 μm where BN dominates (Wynn-Williams et al. 1984). Since H₂O emission is observed on an arcmin scale with the LWS (e.g. Cernicharo et al. 1999a), it is likely that the H₂O covers all of the continuum, at least for the lower-excitation lines. However, the absorption of the lower-lying lines may be partially filled in by emission within the SWS beam. As discussed below, these effects must be taken into account explicitly in an analysis of the equivalent widths.

4. Analysis and discussion

4.1. Spatial origin of the water

It is important to establish where the observed water is located along the line-of-sight towards IRc2. Possible candidates are the quiescent ridge, the shocked (low and/or high velocity)

plateau gas, the hot core, or a combination of these components. Fortunately, our Fabry-Perot observations can aid in resolving the ambiguity. For the 3 pure absorption cases, the v_{LSR} is $\sim -8 \pm 3 \text{ km s}^{-1}$. This blueshift is similar to velocities found for molecules such as CO, C₂H₂ and OCS of -3 to -18 km s^{-1} in absorption by Scoville et al. (1983) and Evans et al. (1991), which they interpret as arising from the low-velocity plateau gas, representing a shell expanding about a point close to IRc2. The most likely candidate for the location of our H₂O gas is therefore the shocked, low-velocity plateau gas. Our lines are also resolved with observed full-width at half-peak $\Delta V \simeq 30 \text{ km s}^{-1}$. Assuming that the intrinsic source profile is Gaussian and that the FP instrumental profile is an ideal Airy profile with FWHM of 10 km s⁻¹, the intrinsic line widths are of order 23 km s⁻¹. This broad linewidth excludes most other components, such as the quiescent ridge and hot core, which have $\Delta V < 20 \text{ km s}^{-1}$ (Blake et al. 1987). H₂O differs in this respect from the other molecules seen in absorption, which have ΔV of order only 3–10 km s⁻¹ (Scoville et al. 1983, Evans et al. 1991).

The peak of the emission component of the 40.69 μm line occurs at $v_{\text{LSR}} = +7$ to $\sim +12 \text{ km s}^{-1}$. This velocity range is similar to that found by Cernicharo et al. (1994) for the 3_{1,3}–2_{2,0} 183 GHz line, as well as for a selection of H₂¹⁸O lines by Zmuidzinas et al. (1995), and is in fact close to $v_{\text{LSR}} \approx 9 \text{ km s}^{-1}$ appropri-

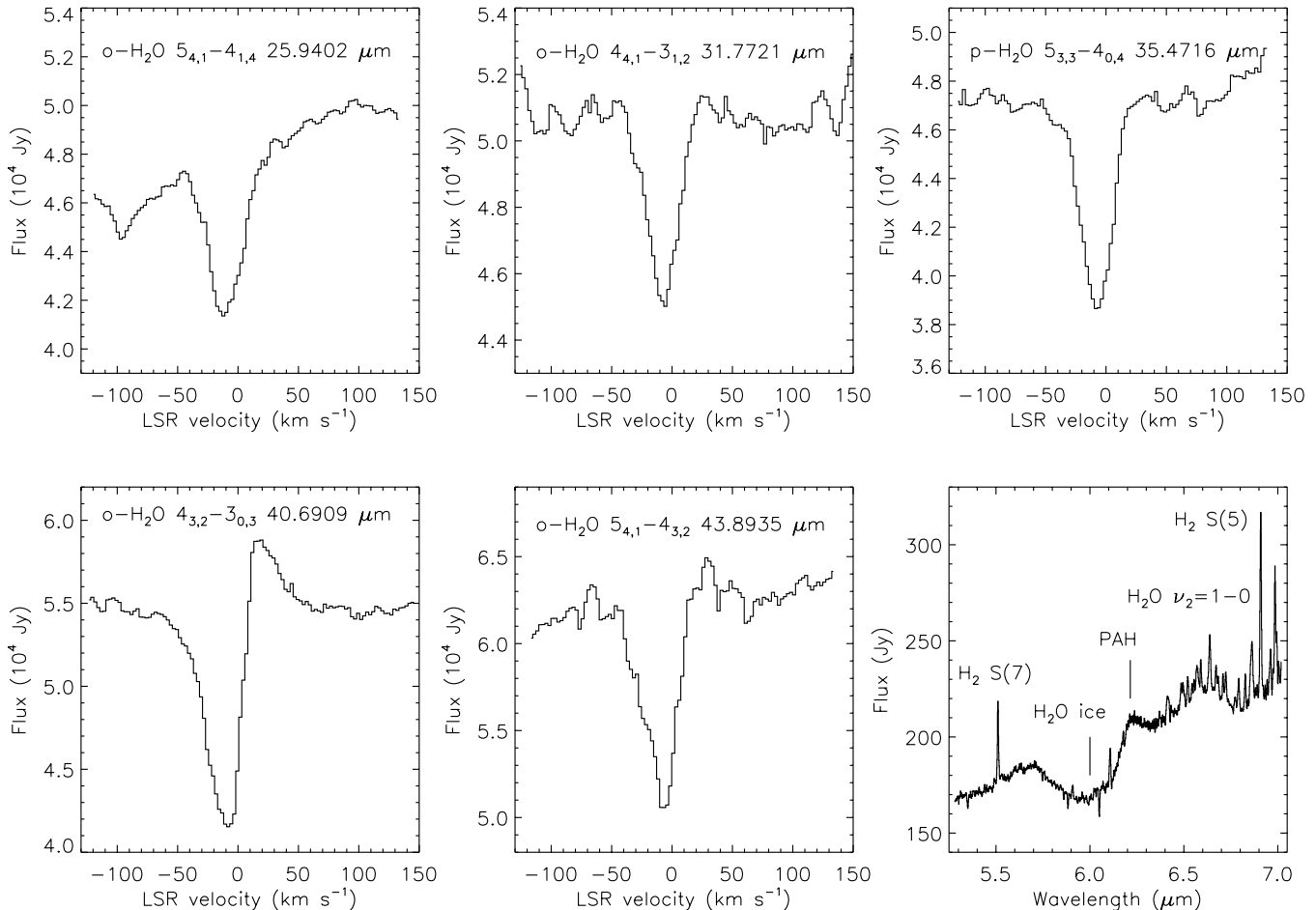


Fig. 3. ISO-SWS Fabry-Perot spectra toward IRc2 of a selection of H₂O absorption lines. The final panel displays the 5.3–7.0 μm grating spectrum of the H₂O $\nu_2=1-0$ band taken simultaneously with the revolution 831 Fabry-Perot spectra.

ate for the dense, quiescent ridge in which IRc2 is embedded. The emission component is also resolved, with an observed linewidth of $\Delta V \approx 40 \text{ km s}^{-1}$, consistent with the intrinsic widths of $\sim 35 \text{ km s}^{-1}$ of the water lines detected in emission at longer wavelengths with the ISO-LWS by Harwit et al. (1998).

In the comparisons presented above the absorbing and emitting components have been considered separately. However, the profile as a whole for the 40.69 μm line, and to some extent also the 43.89 μm line, is very reminiscent of a P Cygni-type profile, and is similar to those observed for several far-infrared OH lines toward Orion by Betz & Boreiko (1989) and Melnick et al. (1990). In fact, the total blue-shift of the absorption component for all 5 lines, i.e. with respect to the rest velocity of the cloud $v_{\text{LSR}} \approx 9 \text{ km s}^{-1}$, is very close to the expansion velocity of the “low-velocity flow”, (or plateau, or “expanding doughnut”) of $18 \pm 2 \text{ km s}^{-1}$ quoted by Genzel et al. (1981) from proper motion studies of the 22 GHz H₂O maser emission. Together with the fact that the emission component of the 40.69 μm line is near the rest velocity of the cloud, this is precisely the definition of a P-Cygni profile and establishes almost without a doubt that the observed water arises from an outflow centered near IRc2, most likely from source “I” (Menten & Reid 1995). As noted by Genzel et al. (1981) this outflow, or low velocity plateau, can

be traced from $\sim 2 \times 10^{17} \text{ cm}$ ($30''$) to within 10^{14} cm from its dynamical center.

We note that Takahashi et al. (1985) predicted that many H₂O lines from a linearly expanding spherical cloud would exhibit P-Cygni type profiles, although the only case in common with our observations, the 40.69 μm line, is not P-Cygni shaped in any of their models. However, they do not include shock emission in their calculations. Further, there is a difference between a true P-Cygni profile and the P-Cygni *type* profiles observed here and predicted by Takahashi et al. A true P-Cygni profile results from an expanding stellar atmosphere *with a central luminosity source*, whilst the P-Cygni type profiles of far-infrared water lines are caused by the presence of warm dust *throughout* the expanding cloud. Further details on water line profiles in regions of intense dust emission may be found in Takahashi et al. (1985) or Doty & Neufeld (1997).

4.2. Excitation of the absorbing water vapour

4.2.1. Generalised curve-of-growth method

The ISO spectra of Orion highlight the need for a non-traditional analysis of interstellar spectra. At shorter wavelengths (in the visible and ultraviolet), molecular absorption lines arise in gas

Table 1. Revolution 660 ISO–SWS H₂O and OH observations toward Orion–IRc2

Wavelength (rest, μm)	Species	Transition $u - \ell$	hcE_{ℓ}/k (K)	W^{obs} (km s^{-1})	W^{GCOG} (km s^{-1})	KN96 ^a (km s^{-1})	τ_0
Grating data – H ₂ O							
25.9402	o-H ₂ O	5 ₄₁ –4 ₁₄	323.49	3.41	2.88	3.4	0.16
27.0272	p-H ₂ O	7 ₃₅ –6 ₀₆	642.69	2.18	2.12	0.01	0.08
27.9903	o-H ₂ O	6 ₄₃ –5 ₁₄	574.73	2.17	1.90		0.07
28.9138	p-H ₂ O	4 ₄₀ –3 ₁₃	204.71	2.58	2.28	1.6	0.10
29.8367	o-H ₂ O	7 ₂₅ –6 ₁₆	643.49	1.44	1.35	0.5	0.07
29.8849	p-H ₂ O	5 ₄₂ –4 ₁₃	396.38	0.82	0.82		0.10
30.8994	o-H ₂ O	6 ₃₄ –5 ₀₅	468.10	3.91	3.98	7.3	0.54
31.7721	o-H ₂ O	4 ₄₁ –3 ₁₂	249.43	2.81	2.83	5.3	0.42
35.4716	p-H ₂ O	5 ₃₃ –4 ₀₄	319.48	3.53	3.61	7.7	1.13
36.2125	p-H ₂ O	6 ₂₄ –5 ₁₅	469.94	1.56	1.57	0.9	0.38
37.9839	o-H ₂ O	4 ₄₁ –4 ₁₄	323.49	0.79	0.11	1.0	0.04
39.3749	o-H ₂ O	5 ₅₀ –4 ₄₁	702.27	1.45	1.60	0.05	0.87
39.3992	p-H ₂ O	6 ₄₂ –5 ₃₃	725.09	0.52	0.52		0.14
40.3368	o-H ₂ O	6 ₄₃ –5 ₃₂	732.06	0.62	0.61	0.15	0.06
40.6909	o-H ₂ O	4 ₃₂ –3 ₀₃	196.77	7.26	7.18	29.8	9.67
40.7597	p-H ₂ O	6 ₃₃ –5 ₂₄	598.83	0.71	0.66	0.04	0.34
43.8935	o-H ₂ O	5 ₄₁ –4 ₃₂	550.35	2.56	2.63	3.7	4.74
44.1946	p-H ₂ O	5 ₄₂ –4 ₃₁	552.26	1.26	1.26	0.18	1.63
45.1116	o-H ₂ O	5 ₂₃ –4 ₁₄	323.49	6.42	6.77	30.9	12.8
Fabry-Perot							
25.9402	o-H ₂ O	5 ₄₁ –4 ₁₄	323.49	4.44	2.88	3.4	
31.7721	o-H ₂ O	4 ₄₁ –3 ₁₂	249.43	3.24	2.83	5.3	
35.4716	p-H ₂ O	5 ₃₃ –4 ₀₄	319.48	5.72	3.61	7.7	
40.6909 ^b	o-H ₂ O	4 ₃₂ –3 ₀₃	196.77	5.20	7.18	29.8	
43.8935 ^c	o-H ₂ O	5 ₄₁ –4 ₃₂	550.35	4.48	2.63	3.7	
Grating data – OH ² $\Pi_{1/2}$ – ² $\Pi_{3/2}$, $N, J =$							
28.93461	OH	4, $\frac{7}{2}e, f$ –2, $\frac{5}{2}e, f$	120.46	2.86			
34.59617	OH	3, $\frac{5}{2}f$ –1, $\frac{3}{2}f$	0.08	4.46			
34.62215	OH	3, $\frac{5}{2}e$ –1, $\frac{3}{2}e$	0.00	4.68			

^a Orion shock model of Kaufman & Neufeld (1996), using lower oxygen and H₂O abundances of 3.16×10^{-4} and 3.5×10^{-4} respectively, cf. Harwit et al. (1998), and assuming a shock velocity of 37 km s^{-1} .

^b The net equivalent width, including both emission and absorption components. Individually, the observed absorption component is 11.07 km s^{-1} , whilst the emission component flux is $7.8 \times 10^{-18} \text{ W cm}^{-2}$.

^c The net equivalent width, including both emission and absorption components. Individually, the observed absorption component is 6.11 km s^{-1} , whilst the emission component flux is $2.3 \times 10^{-18} \text{ W cm}^{-2}$.

that is physically very cold in relation to the radiation temperature of the background star, so that the absorption can be described with a classical curve-of-growth analysis and the effects of stimulated emission can be neglected. At longer wavelengths (radio), an isolated molecular region typically exhibits collisionally excited emission lines on top of a weak continuum so that the most significant radiative coupling is to the cosmic background radiation at $T_{\text{cbr}} = 2.728 \text{ K}$. In the present case, we observe a molecular spectrum that is formed in the presence of a very strong continuum, i.e., where the radiation temperature of the continuum may be comparable to the excitation energies of the states involved. This implies both that the classical curve-of-growth analysis of cold absorbers detached from the background continuum is invalid and that the standard analysis of collisional excitation in competition with a very cold,

dilute background is inadequate. Indeed, it is the near equality of continuum brightness temperature $T_{\text{rad}}(\nu)$ and molecular excitation temperature T_{ex} that explains at least partly why the water spectrum of Orion IRc2 is predominantly in absorption at $\lambda \lesssim 50 \mu\text{m}$ and in emission at longer wavelengths. In detail, such spectra should be modelled as an extended atmosphere in which lines and continuum are treated consistently. We will outline briefly how it is possible to extract important information on excitation and abundance through a simpler analysis of the unresolved lines based on a generalised curve-of-growth. Details of this method will be discussed elsewhere (Black, in preparation).

Consider the situation in which a fractional area a_c of a continuum source of intensity $I_c(\nu)$ is obscured by a column of gas in the foreground. The observed spectrum in the vicinity

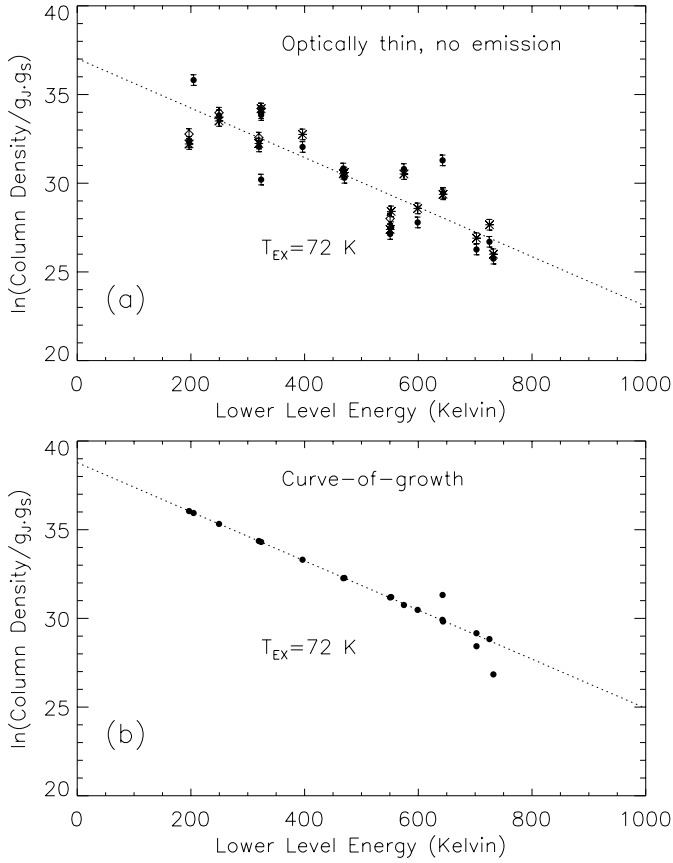


Fig. 4. **a** Level populations of H₂O derived from the absorption lines and using the optically thin formula $N_\ell = (8\pi c W_\lambda g_\ell) / (\lambda^4 A_{ul} g_u)$. The solid circles represent the revolution 660 grating data, the asterisks the revolution 826 grating data, and the open diamonds the revolution 823 and 831 Fabry-Perot data. The dotted line represents a best fit 1st order polynomial to the revolution 660 data, and implies an excitation temperature of 71.6 K. A similar fit to the revolution 826 data yields 75.9 K, whilst the Fabry-Perot absorption (emission) data yield 62.9 K (64.4 K). **b** Level populations of H₂O derived from the generalised curve-of-growth (GCOG) analysis of the revolution 660 data. The best fit GCOG analysis for the populations results in a distribution that is consistent with a thermal distribution at a constant excitation temperature of 72.5 K. The dotted line indicates a best fit 1st order polynomial to the points with $E_\ell < 600$ K.

of a transition $u \leftrightarrow \ell$ is given by the sum of the unattenuated continuum (first term), the absorbed continuum (second term), and the emission of the cloud itself (third term):

$$I_{\text{obs}}(\nu) = (1 - a_c)I_c(\nu) + a_c I_c(\nu) e^{-\tau_{u\ell}(\nu)} + B_\nu(T_{u\ell}) \left(1 - e^{-\tau_{u\ell}(\nu)}\right), \quad (1)$$

where $\tau_{u\ell}$ is the optical depth and $B_\nu(T_{u\ell})$ is the Planck function evaluated for an excitation temperature $T_{u\ell}$. This temperature is defined by the column densities of molecules in the upper (N_u) and lower (N_ℓ) states through:

$$\frac{N_u}{N_\ell} = \frac{g_u}{g_\ell} \exp\left(-\frac{h\nu}{kT_{u\ell}}\right). \quad (2)$$

The optical depth function for a single line can be written (e.g. Rybicki & Lightman 1979, Wannier et al. 1991)

$$\tau_{u\ell}(\nu) = 3.738 \times 10^{-7} \frac{A_{ul}}{\tilde{\nu}_{ul}^3} \frac{N_\ell g_u}{\Delta V g_\ell} \times \left(1 - \exp\left(-\frac{h\nu}{kT_{u\ell}}\right)\right) \phi(\nu) \quad (3)$$

where N_ℓ is in cm⁻², $\tilde{\nu}_{ul} = \nu_{u\ell}/c$ is the wavenumber of the line in cm⁻¹, and the line shape function is a gaussian of full-width at half-maximum ΔV in km s⁻¹, normalized so that $\phi(\nu_{u\ell}) = 1.0$. The term in parentheses is the correction for stimulated emission.

The generalised equivalent width, in frequency units, is expressed as

$$W_\nu^{\text{obs}} = \int \frac{I_c(\nu) - I_{\text{obs}}(\nu)}{I_c(\nu)} d\nu \quad (4a)$$

$$W_\nu^{\text{obs}} = \int \left[\left(a_c - \frac{B_\nu(T_{u\ell})}{I_c(\nu)} \right) \left(1 - e^{-\tau_{u\ell}(\nu)} \right) \right] d\nu. \quad (4b)$$

In the limit as $a_c \sim 1$ and $T_{u\ell} \ll h\nu/k$, the equivalent width approaches the classical form of cold absorbers detached from the background continuum. By convention, the equivalent width is positive for net absorption and negative for emission. Emission can arise either when $T_{u\ell}$ is large enough that $B_\nu(T_{u\ell})/I_c(\nu) > a_c$ or when there is a population inversion ($N_u/N_\ell > g_u/g_\ell$) so that $\tau_{u\ell}$ is negative, as in a maser.

For a single unresolved line of equivalent width W_ν^{obs} , there is not a unique solution, because 4 parameters must be constrained: a_c , N_u , N_ℓ , and ΔV . In the classic problem, in which a continuum point source of intensity is located behind, and completely obscured by, a column of cold foreground gas, and there is negligible population in the upper level of an absorption transition, then $a_c = 1$ and $N_u/N_\ell \sim 0$ respectively. In that case, two lines arising in a common level suffice to determine N_ℓ and ΔV .

4.2.2. Results of the generalised curve-of-growth analysis

We have analyzed the equivalent widths using Eq. (4b). If we take the continuum intensity to be approximately constant over the line profile, then the term $a_c - B_\nu(T_{u\ell})/I_c(\nu)$ can be taken outside the integral in Eq. (4b). We adopt an empirical continuum intensity $I_c(\nu) = f_\nu^{\text{obs}}/\Omega_{\text{beam}}$, where f_ν^{obs} is the flux density observed in the ISO–SWS aperture of solid angle Ω_{beam} . When $I_c(\nu)$ is fixed in this way, the equivalent width of a line depends on the parameters N_ℓ , $T_{u\ell}$, ΔV , and a_c . We adopt an intrinsic width $\Delta V = 23$ km s⁻¹ and assume that a_c has the same value for all lines in the following analysis. Thus each line is characterized by two parameters N_ℓ and $T_{u\ell}$ (or N_ℓ and N_u). The solution is still underdetermined because there are 29 distinct energy states involved in the 19 observed transitions. Fortunately, there are several cases in which some of the same states are involved in two or more transitions. As a first approximation, it is assumed that a single value of the excitation temperature $T_{u\ell} = T_{\text{ex},0}$ applies to all transitions with lower-state energies $E_\ell \leq 275$ cm⁻¹. The computed equivalent widths

(Eq. 4b) agree with the observed values within 33% for all but the weakest one of these lines, when $a_c = 1$, $T_{\text{ex},0} = 72.5$ K, and $N_{\text{total}} = 1.5 \times 10^{18} \text{ cm}^{-2}$. This solution is not very sensitive to the value of the continuum covering factor: for $a_c = 0.9$, we obtain $T_{\text{ex},0} = 71.0$ K and $N_{\text{total}} = 1.6 \times 10^{18} \text{ cm}^{-2}$, while for $a_c = 0.8$, the corresponding results are 69.1 K and $1.7 \times 10^{18} \text{ cm}^{-2}$.

With the populations of the lowest energy states ($E_\ell \leq 275 \text{ cm}^{-1}$) fixed at $T_{\text{ex},0} = 72.5$ K, the column densities in higher states are adjusted until the standard deviation of the mean $W^{\text{obs}} - W^{\text{GCOG}}$ is minimized for the entire set of lines. In this solution, the observed W^{obs} and calculated W^{GCOG} equivalent widths all agree within 16%, with the single exception of the $4_{41} - 4_{14}$ line at $37.98 \mu\text{m}$. The calculated equivalent widths are listed in Table 1. Note that the adjustment also improves the fit for the lines arising in the low-lying states because W^{GCOG} is sensitive to column densities in both the upper and lower states. The result is a population distribution that is indistinguishable from a thermal distribution at 72.5 K for all states with $hcE_i/k \lesssim 700$ K. A few of the observed levels at higher energies ($hcE_i/k > 700$ K) are well constrained because they are the upper states of more than one transition, and their populations start to clearly show effects of subthermal excitation, $T_{ul} \approx 55$ K. Even though the adopted linewidth is large, the derived line-center optical depths, listed in Table 1, reach values as high as $\tau_0 = 12.8$ and 9.7 in the 45.11 and $40.69 \mu\text{m}$ lines, respectively. The smallest values of optical depth are $\tau_0 \approx 0.06$. Finally, ortho and para states of H_2O are consistent with the same excitation temperature and with an ortho/para ratio of 3.

The results of our generalised curve-of-growth analysis are shown graphically in Fig. 4(b), in the form of a standard population diagram. The much reduced scatter in the data is clearly a marked improvement over the optically thin approach assuming no stimulated emission used in obtaining Fig. 4(a). It is however interesting that the inferred excitation temperatures from the two approaches are similar. The excitation temperature of ~ 72 K is similar to the colour temperature of the dust between 20 and $100 \mu\text{m}$ inferred by Werner et al. (1976), which confirms the expectation that pumping by infrared continuum radiation from dust plays an important role in the H_2O excitation. In this case, there is no direct constraint on the kinetic temperature of the H_2O -containing gas. Subthermal excitation by collisions at densities below the critical densities of the observed levels ($\sim 10^9 \text{ cm}^{-3}$) can also result in excitation temperatures of order 50–100 K, but this merely re-affirms that radiative processes probably dominate the excitation. We also note that the excitation temperature inferred from the emission components of the 40.69 and $43.89 \mu\text{m}$ lines is ~ 64 K, also implying a large contribution by radiative processes to the populations. Moreover, the analysis suggests that T_{ul} of the absorption lines is so close to the continuum radiation temperature in this wavelength range, that it is easy to see why the H_2O spectrum should go into emission at $\lambda > 50 \mu\text{m}$ as the opacity and radiation temperature of the continuum decrease with increasing wavelength.

Because the lowest state involved in the $25\text{--}45 \mu\text{m}$ spectrum lies at $hcE_i/k = 197$ K, we cannot determine the column

densities in the most populated states directly from these observations. However, if we assume that the observed excitation pattern applies to the unobserved lower states, then we infer a total column density of $N(\text{H}_2\text{O}) = 1.5 \times 10^{18} \text{ cm}^{-2}$ averaged over the ISO–SWS beam toward Orion IRc2.

The net absorption by water in Orion is sensitive to the competition between the molecular excitation and the continuum brightness. We have assumed that the true continuum intensity in Eq. (4) is equal to the mean surface brightness observed in the spectrum (flux averaged over the aperture). In general this need not be true, and the analysis can include an additional correction factor for the coupling to the continuum. Tests show that if the continuum intensity is thus changed by a factor of two in either direction, the derived total column density and mean excitation temperature change by less than 20%, which we take as our maximum uncertainty.

4.2.3. Shock models

We have also compared our observed line equivalent widths with those computed for the Kaufman & Neufeld (1996) C-shock in Orion with a pre-shock density of 10^5 cm^{-3} and shock velocity of 37 km s^{-1} (Kaufman & Neufeld, private communication) (see Table 1). The water abundance (with respect to H_2) used in this shock calculation was 3.5×10^{-4} , based on the O and C abundances of Cardelli et al. (1996), with all the carbon locked up in CO and H_2O accounting for all the remaining oxygen. Although this model refers to “peak 1” rather than the IRc2 region, it reproduces the equivalent widths quite well within a factor of a few, except for some of the higher-lying lines (e.g., 27.03 , 39.37 , 40.76 , $44.19 \mu\text{m}$). Most of these lines are likely to be strongly affected by radiative excitation, which was not included in their model.

We note that the shock velocity used is 37 km s^{-1} , different from the expansion velocity inferred from our FP observations of 18 km s^{-1} . Indeed, our modelling of our H_2 emission, using the Kaufman & Neufeld (1996) shock model, indicates that at least 2 shock components are required. One component at $15\text{--}20 \text{ km s}^{-1}$ matches well the observed column densities in the $v=0$, $J=3$ to 7 levels, whilst a second component, at 35 km s^{-1} , is required to match higher J levels and the ro-vibrational lines (Wright 1999). Harwit et al. (1998) used a shock velocity of 37 km s^{-1} to match their 8 LWS water line emission detections from 72 to $125 \mu\text{m}$. These data were taken at a slightly different position, centred on BN rather than IRc2 and offset $8.2''$ to the north. The SWS results may therefore be more sensitive to the low-velocity plateau gas identified by several authors (e.g. Genzel & Stutzki 1989), whereas the larger LWS beam will include a significant contribution from the high-velocity gas. We also note that water line emission in the Kaufman & Neufeld (1996) shock models is for many lines insensitive to the shock velocity, especially when the velocity is $\geq 15\text{--}20 \text{ km s}^{-1}$. This is presumably because in such cases the water abundance has reached its maximum value and that the gas temperature is well above the upper levels involved. Therefore, the emission depends more on density and not temperature (which in turn is highly sensitive

to the shock velocity). Even so, future attempts to match both the Harwit et al. lines and our detections with a slower shock, but including radiative excitation, will be worthwhile.

A long standing problem in shock research is the contribution of water to the total gas cooling behind the shock, and it is pertinent to mention it here. Unfortunately, the situation in Orion IRc2, i.e. a high water abundance (see Sect. 4.3) coupled with an intense mid- and far-infrared radiation field, has not previously been considered in shock models. However, the detection of all our transitions in absorption raises the interesting possibility that at least these transitions are not cooling the gas, but rather heating it. Such heating results from the water molecules absorbing the radiation and thereby being raised to excited states. The excess energy may then be imparted to the gas through collisional de-excitation with other molecules, e.g. H_2 , as in the scenario proposed by Takahashi et al. (1983). This would of course be in competition with radiative de-excitation (i.e. cooling), and is therefore density dependent. Further, Takahashi et al. (1983) and Neufeld et al. (1995) state that a necessary condition for H_2O heating is that the dust temperature is greater than the gas temperature. A full scale shock model, taking into account all transitions, would be required to determine if there was net heating or cooling. We merely mention it here as an interesting aside, and direct the reader to the paper by Harwit et al. (1998) for a full discussion of the water cooling contribution in Orion. Briefly though, from their larger beam LWS observations they find that H_2O and CO contribute similar amounts to the overall cooling, but both are only about a tenth of the total H_2 cooling. On the other hand, Saraceno et al. (1999), in a study of a sample of shock sources, find that CO cooling typically dominates over H_2O by a factor of several.

4.3. H_2O abundance in Orion

In order to determine an H_2O abundance directly from our data, information on the H_2 column density is needed. As noted above, from the H_2 lines detected elsewhere in our spectra (van Dishoeck et al. 1998), the shock has been characterized using the Kaufman & Neufeld (1996) C-shock models, in a manner similar to that applied by Wright et al. (1996) to Cepheus A. Further details can be found in Wright (1999); in short, the H_2 pure rotational lines originating from $J=3$ to $J=7$ indicate a column $N(\text{H}_2)=(1.2 \pm 0.2) \times 10^{21} \text{ cm}^{-2}$ of warm ($T_{ex}=700 \text{ K}$) gas, and the inferred shock velocity of $15\text{--}20 \text{ km s}^{-1}$ is similar to the 18 km s^{-1} expansion velocity deduced from our FP observations, but lower than that obtained from modeling the H_2 vibration-rotation lines (35 km s^{-1}). However, supporting evidence for the co-location of the H_2O and shocked H_2 comes from Scoville et al. (1982), who find that at and around the position of IRc2 the peak emission of the $1\text{--}0 \text{ S}(1)$ line is at $v_{\text{LSR}}=-6$ to -16 km s^{-1} , similar to the velocity of maximum H_2O absorption in our spectra.

Using the above H_2 column density, and that of H_2O calculated from the generalised curve-of-growth analysis, the inferred water abundance would be 1.25×10^{-3} . However, the inferred column density from the high- J (i.e. 3–7) lines is a

lower limit on the total column density, since the bulk of the H_2 is likely to be cooler than $T_{ex}=700 \text{ K}$. Such cooler gas would be probed by the $28.2 \mu\text{m}$ H_2 0–0 S(0) line, but which unfortunately has not been detected toward IRc2, due to the extremely high continuum emission. However, a lower limit implies that $T_{ex} \geq 110 \text{ K}$, calculated from the populations in $J=3$ and 2, inferred from the observed 0–0 S(1) and upper limit S(0) lines respectively. On the other hand, the S(0) line is detected at about the 3σ level toward the shock “peak 2”, $\sim 30''$ to the south-east of IRc2, and in this case the excitation temperature between the $J=3$ and $J=2$ levels is $\sim 150 \text{ K}$ (Wright 1999).

This temperature of $\sim 150 \text{ K}$ is likely to be indicative of the kinetic temperature, T_{kin} , at this position, since the density of $\geq 10^5 \text{ cm}^{-3}$ (e.g. Genzel & Stutzki 1989) is above the critical density of the H_2 0–0 S(0) and S(1) transitions (e.g. Le Boulart et al. 1999). Although this estimate of T_{kin} is at a different position than where the water absorption line detections were made, Wright (1999) shows that in at least 3 shock sources, including Orion, the excitation temperature determined from pure rotational H_2 lines ($J_{up}=3\text{--}7$) is quite invariant across the sources, as is the column density. Other estimates of T_{kin} in the low-velocity plateau, tabulated by Genzel & Stutzki (1989), range from 100–500 K.

If we assume that T_{kin} is between 100–500 K, then Table 2 presents the expected total H_2 column density based on the observed surface brightness of the 0–0 S(1) line toward IRc2 of $1.5 \times 10^{-10} \text{ W cm}^{-2} \text{ sr}^{-1}$. We believe that 100 K is too low to be applicable to the shocked plateau gas, since it is lower than T_{kin} we find at “peak 2”, and in any case would imply a column density an order of magnitude larger than the value of 10^{23} cm^{-2} quoted by Genzel & Stutzki (1989). Also shown in Table 2 is the inferred water abundance, $N(\text{H}_2\text{O})/N(\text{H}_2)$, using the observed water column density of $1.5 \times 10^{18} \text{ cm}^{-2}$, and assuming the water and molecular hydrogen to be co-located. Taking the maximum possible water abundance to be 5×10^{-4} (anything higher would violate the constraint imposed by the oxygen abundance itself of $[\text{O}]/[\text{H}]=3.19 \times 10^{-4}$ from Meyer et al. 1998), then the water abundance is in the range of $2.6\text{--}50 \times 10^{-5}$.

Let us instead assume *a priori* that our water detections arise only in that portion of the shock where the temperature is high enough for the water creation reactions to rapidly proceed. Several authors (e.g. Hollenbach & McKee 1979, Neufeld et al. 1995, Ceccarelli et al. 1997 and Charnley 1997) have shown that water begins to be quickly formed when the temperature exceeds about 230 K, and has reached its maximum abundance by about 320 K. In that case our inferred water abundance is in the range $2\text{--}5 \times 10^{-4}$, in remarkable agreement with the result of Harwit et al. (1998) of $3.5\text{--}5 \times 10^{-4}$ considering the different methods used. Further, it is interesting to note that Watson et al. (1985) find a H_2 column density of $3 \times 10^{21} \text{ cm}^{-2}$, derived from several observed far-infrared CO lines in a $44''$ beam, implying a H_2O abundance of 5×10^{-4} . Watson et al. however infer a kinetic temperature of 750 K, close to the excitation temperature derived from our H_2 data (Wright 1999), whereas from Table 2

Table 2. Inferred total H₂ column densities and water abundances

T_{kin} (Kelvin)	$N(\text{H}_2)^a$ (cm ⁻²)	$N(\text{H}_2\text{O})/N(\text{H}_2)^b$
100	1.1×10^{24}	1.4×10^{-6}
150	5.7×10^{22}	2.6×10^{-5}
200	1.4×10^{22}	1.1×10^{-4}
230	8.1×10^{21}	1.9×10^{-4}
250	6.2×10^{21}	2.4×10^{-4}
280	4.4×10^{21}	3.4×10^{-4}
300	3.7×10^{21}	4.1×10^{-4}
320	3.2×10^{21}	4.7×10^{-4}
350	2.6×10^{21}	5.8×10^{-4}
400	2.1×10^{21}	7.1×10^{-4}
450	1.7×10^{21}	8.8×10^{-4}
500	1.5×10^{21}	1.0×10^{-3}

^a Assuming that the observed H₂ 0–0 S(1) 17.0348 μm line, with surface brightness 1.5×10^{-10} W cm⁻² sr⁻¹, arises from gas with kinetic temperature T_{kin} .

^b Using a total water column density of 1.5×10^{18} cm⁻², and assuming the H₂ and H₂O are co-located.

their column density would instead imply a temperature of only ~330 K.

Alternatively, if we simply use a H₂ column density of 10^{23} cm⁻² for the plateau gas, as given by Genzel & Stutzki (1989), then the water abundance is 1.5×10^{-5} , in better agreement with that of other shocks (e.g. Liseau et al. 1996, Ceccarelli et al. 1998, Spinoglio et al. 1999), and suggesting that a substantial fraction of the gas-phase oxygen may still be in another form, most likely gas-phase atomic O I. However, this is probably a strict lower limit, since such a large column density probably includes gas at a temperature lower than 230 K, as well as gas behind the infrared continuum source.

An H₂O abundance at the high end of the range quoted above, i.e. $2\text{--}5 \times 10^{-4}$, is favored if we assume that water is only efficiently created in regions where the temperature is greater than about 230 K. This water abundance is consistent with all of the gas-phase oxygen not locked up in CO being incorporated into H₂O. However, H₂O ice evaporates at temperatures above about 90 K, so lower temperatures, and hence a lower abundance, cannot be excluded. The major uncertainty on our abundance value is the total hydrogen column density. As mentioned above, our result is in good agreement with Harwit et al. (1998), but also in agreement with Cernicharo et al. (1999a,b) from LWS and ground based observations respectively. From radiative transfer modelling of their water detections, they find toward the Orion plateau a water abundance of order $1\text{--}2 \times 10^{-4}$, at most a factor of a few lower than what we find. Besides Orion, there is only one other source so far observed by ISO with such a high water abundance, namely L1448-mm by Nisini et al. (1999), with an abundance of order 5×10^{-4} .

A similar treatment for the OH lines detected in our spectrum yields a column density of approximately 5×10^{16} cm⁻², after fixing T_{ex} to be the same as that for water. The implied OH

abundance is then $(8.8\text{--}156) \times 10^{-7}$ for $T_{kin}=150\text{--}320$ K, or $(6.2\text{--}15.6) \times 10^{-6}$ for 230–320 K.

5. Conclusions

Through use of the ISO-SWS in its grating mode, 19 pure rotational absorption lines of water have been detected toward Orion IRc2 for the first time. Fabry-Perot spectra of 5 lines reveal that the water is located in an outflow expanding at a velocity of 18 km s⁻¹. The strong mid-infrared continuum toward IRc2 plays a dominant role in the excitation of the molecule and the line formation, which can be modeled using a simple, generalised curve-of-growth technique. This yields a total water column density of order 1.5×10^{18} cm⁻² and excitation temperature of 72 K, similar to the dust continuum colour temperature. Both derived quantities have a maximum uncertainty of about 20%. The data provide support for large abundances of H₂O in the outflows of massive stars. Simultaneous analysis of the complete ISO-SWS and LWS data set on H₂O, OH and CO may provide further information on the abundance and excitation of these molecules in the various physical components within the complex Orion environment.

Acknowledgements. The authors are grateful to the SWS instrument teams in Groningen and Garching and to the SIDT in Vilspa for making these observations possible. They are indebted to G.A. Blake, A. Boonman, F. van der Tak, G.J. Melnick, A.G.G.M. Tielens and R. Timmermann for useful discussions. They are especially grateful to D.A. Neufeld and M.J. Kaufman for providing them with the equivalent widths of the H₂O lines in their models, and to W.F. Thi for developing the code for the up-down scan correction. This work was supported by NWO grant 614.41.003 and by the Spanish DGES grant PB96-0883 and PNIE grant ESP97-1618-E. During the final phases of this work CMW was supported by an ARC Australian Postdoctoral Research Fellowship.

References

- Beckwith S., Persson S.E., Neugebauer G., Becklin, E.E., 1978, ApJ 223, 464
- Betz A.L., Boreiko R.T., 1989, ApJ 346, L101
- Blake G.A., 1997, In: van Dishoeck E.F. (ed.) *Molecules in Astrophysics: Probes and Processes*. IAU Symposium 178, Kluwer, Dordrecht, p. 31
- Blake G.A., Sutton E.C., Masson C.R., Phillips T.G., 1987, ApJ 315, 621
- Cardelli J.A., Meyer D.M., Jura M., Savage B.D., 1996, ApJ 467, 334
- Ceccarelli C., Hollenbach D.J., Tielens A.G.G.M., 1997, ApJ 471, 400
- Ceccarelli C., Caux E., White G.J., et al., 1998, A&A 331, 372
- Cernicharo J., González-Alfonso E., Alcolea J., Bachiller R., John D., 1994, ApJ 432, L59
- Cernicharo J., Lim T., Cox P., et al., 1997a, A&A 323, L25
- Cernicharo J., González-Alfonso E., Lefloch B., 1997b, In: Heras A., et al. (eds.) *First ISO workshop in Analytical Spectroscopy*. ESA SP-419, ESTEC, Noordwijk, p. 23
- Cernicharo J., González-Alfonso E., Sempere M.J., et al., 1999a, In: Cox P., Kessler M.F. (eds.) *The Universe as seen by ISO*. ESA Publications Division SP-427, ESTEC, Noordwijk, p. 565

- Cernicharo J., Pardo J.R., González-Alfonso E. et al., 1999b, *ApJ* 520, L131
- Charnley S.B., 1997, *ApJ* 481, 396
- Cheung A.C., Rank D.M., Townes C.H., et al., 1969, *Nat* 221, 626
- Dartois E., d'Hendecourt L., Boulanger F., et al., 1998, *A&A* 331, 651
- de Graauw Th., Haser L.N., Beintema D.A., et al., 1996, *A&A* 315, L49
- Downes D., Genzel R., Becklin E.E., Wynn-Williams C.G., 1981, *ApJ* 244, 869
- Doty S.D., Neufeld D.A., 1997, *ApJ* 489, 122
- Evans N.J., Lacy J.H., Carr J.S., 1991, *ApJ* 383, 674
- Feuchtgruber H., Lutz D., Beintema D.A., et al., 1997, *ApJ* 487, 962
- Gensheimer P.D., Mauersberger R., Wilson T.L., 1996, *A&A* 314, 281
- Genzel R., Reid M.J., Moran J.M., Downes D., 1981, *ApJ* 244, 884
- Genzel R., Stutzki J., 1989, *ARA&A* 27, 41
- Goldsmith P.F., Langer W.D., 1999, *ApJ* 517, 209
- González-Alfonso E., Cernicharo J., van Dishoeck E.F., Wright C.M., Heras A., 1998, *ApJ* 502, L169
- Harwit M., Neufeld D.A., Melnick G.J., Kaufman M.J., 1998, *ApJ* 497, L105
- Heras A.M., 1997, In: Heras A.M., Leech K., Trams N.R., Perry M. (eds.) *First ISO Workshop on Analytical Spectroscopy*. ESA Publications Division SP-419, Noordwijk, p. 271
- Hollenbach D.J., McKee C.F., 1979, *ApJS* 41, 555
- Jacq T., Walmsley C.M., Henkel C., et al., 1990, *A&A* 228, 447
- Kaufman M.J., Neufeld D.A., 1996, *ApJ* 456, 611
- Le Boulrot J., Pineau des Forêts G., Flower D.R., 1999, *MNRAS* 305, 802
- Liseau R., Ade P., Armand C., et al., 1996, *A&A* 315, L181
- Melnick G.J., Stacey G.J., Genzel R., Lugten J.B., Poglitsch A., 1990, *ApJ* 348, 161
- Menten K.M., Reid M.J., 1995, *ApJ* 445, L157
- Meyer D.M., Jura M., Cardelli J.A., 1998, *ApJ* 493, 222
- Neufeld D.A., Melnick G.J., 1987, *ApJ* 322, 266
- Neufeld D.A., Melnick G.J., 1991, *ApJ* 368, 215
- Neufeld D.A., Lepp S., Melnick G.J., 1995, *ApJS* 100, 132
- Nisini B., Benedettini M., Giannini T., et al., 1999, *A&A* 350, 529
- Phillips T.G., Scoville N.Z., Kwan J., Huggins P.J., Wannier P.G., 1978, *ApJ* 222, L59
- Rybicki G.B., Lightman A.P., 1979, *Radiative Processes in Astrophysics*. Wiley
- Saraceno P., Benedettini M., Di Giorgio A.M., et al., 1999, In: Ossenkopf V., et al. (eds.) *The Physics and Chemistry of the Interstellar Medium. The 3rd Cologne-Zermatt Symposium*, GCA-Verlag Herdecke, p. 279
- Schaeidt S.G., Morris P.W., Salama A., et al., 1996, *A&A* 315, L55
- Scoville N.Z., Hall D.N.B., Kleinmann S.G., Ridgway S.T., 1982, *ApJ* 253, 136
- Scoville N.Z., Kleinmann S.G., Hall D.N.B., Ridgway S.T., 1983, *ApJ* 275, 201
- Spinoglio L., Giannini T., Saraceno P., et al., 1999, In: Cox P., Kessler M.F. (eds.) *The Universe as seen by ISO*, ESA Publications Division SP-427, ESTEC, Noordwijk, p. 517
- Takahashi T., Hollenbach D.J., Silk J., 1983, *ApJ* 275, 145
- Takahashi T., Hollenbach D.J., Silk J., 1985, *ApJ* 292, 192
- Tauber J., Olofsson G., Pilbratt G., Nordh L., Frisk U., 1996, *A&A* 308, 913
- Timmermann R., Poglitsch A., Nikola T., Geis N., 1996, *ApJ* 460, L65
- Valentijn E.A., Feuchtgruber H., Kester D.J.M., et al., 1996, *A&A* 315, L60
- van Dishoeck E.F., 1998, *Faraday Disc.* 109, 31
- van Dishoeck E.F., Helmich F.P., 1996, *A&A* 315, L177
- van Dishoeck E.F., Wright C.M., Cernicharo J., et al., 1998, *ApJ* 502, L173
- Wannier P.G., Pagani L., Kuiper T.B.H., et al., 1991, *ApJ* 377, 171
- Waters J.W., Gustinic J.J., Kakar R.K., et al., 1980, *ApJ* 235, 57
- Watson D.M., Genzel R., Townes C.H., Storey J.W.V., 1985, *ApJ* 298, 316
- Werner M.W., Gatley I., Harper D.A., et al., 1976, *ApJ* 204, 420
- Wright C.M., 1999, In: Minh Y.C., van Dishoeck E.F. (eds.) *Astrochemistry: From Molecular Clouds to Planetary Systems*. Proceedings of the IAU Symposium 197
- Wright C.M., Drapatz S., Timmermann R., et al., 1996, *A&A* 315, L301
- Wright C.M., van Dishoeck E.F., Helmich F.P., et al., 1997, In: Heras A., et al. (eds.) *First ISO workshop on Analytical Spectroscopy*. ESA SP-419, ESTEC, Noordwijk, p. 37
- Wynn-Williams C.G., Genzel R., Becklin E.E., Downes D., 1984, *ApJ* 281, 172
- Zmuidzinas J., Blake G.A., Carlstrom J., et al., 1995, In: Haas M.R., Davidson J.A., Erickson E.F. (eds.) *Proceedings of the Airborne Astronomy Symposium on the Galactic Ecosystem: from Gas to Stars to Dust*. ASP, San Francisco, p. 33